12-7-2010

Optimization Design of Electrodes for Anode-Supported Solid Oxide Fuel Cells via Genetic Algorithm

Junxiang Shi

Xingjian Xue
University of South Carolina - Columbia, xue@cec.sc.edu

Publication Info

Published in *Journal of The Electrochemical Society*, Volume 158, Issue 2, 2010, pages B143-B151.

Publisher's Version: http://dx.doi.org/10.1149/1.3517476
Shi, J. & Xue, X. (7 December 2010). Optimization Design of Electrodes for Anode-Supported Solid Oxide Fuel Cells via Genetic Algorithm. Journal of The Electrochemical Society, 158 (2), B143 – B151. http://dx.doi.org/10.1149/1.3517476

Journal of The Electrochemical Society, **158** (2) B143-B151 (2011) B143
0013-4651/2010/158(2)/B143/9/$28.00 © The Electrochemical Society

Optimization Design of Electrodes for Anode-Supported Solid Oxide Fuel Cells via Genetic Algorithm

Junxiang Shi and Xingjian Xue[z]

Department of Mechanical Engineering, University of South Carolina, Columbia, South Carolina 29208, USA

Porous electrode is the critical component of solid-oxide fuel cells (SOFCs) and provides a functional material backbone for multi-physicochemical processes. Model based electrode designs could significantly improve SOFC performance. This task is usually performed via parameter studies for simple case and assumed property distributions for graded electrodes. When nonlinearly coupled multiparameters of electrodes are considered, it could be very difficult for the model based parameter study method to effectively and systematically search the design space. In this research, the optimization approach with a genetic algorithm is demonstrated for this purpose. An anode-supported proton conducting SOFC integrated with a fuel supply system is utilized as a physical base for the model development and the optimization design. The optimization results are presented, which are difficult to obtain for parametric study method.
 [DOI: 10.1149/1.3517476]

Manuscript submitted July 16, 2010; revised manuscript received October 19, 2010. Published December 7, 2010.

Solid oxide fuel cell (SOFC) has been widely recognized as one of the promising clean energy technologies. Porous electrode is a critical component of SOFCs and provides a functional material backbone for electrochemical reactions, charge migrations, fuel/gas species transport, and heat transfer. As a result, the microstructure properties of porous electrodes significantly affect the SOFC performance, such as activation overpotentials and concentration overpotentials. In order to understand the fundamental mechanisms associated with multi-physicochemical processes in porous electrodes, mathematical modeling approach has been extensively employed in literatures, where the model parameters associated with electrodes are characterized using a spherical particle random packing method.[1-7] Upon mathematical model development, parameter studies are utilized to improve electrode performance. Ni et al.[5] investigated effects of electrode porosity, the porosity value of 0.4 identified can maximize cell performance under certain operating conditions. Nam and Jeon[6,7] found that particle diameter is the most important parameter determining cell performance, e.g., smaller particles may lead to the reduced activation overpotential loss, the increased triple phase boundary (TPB) length, and the increased concentration overpotential losses. Their studies also indicated that the porosity and thickness of electrodes have the conflicting effects on the cell performance. In this context, homogeneous electrode property is generally assumed.

Functionally graded electrode has shed light on the novel electrode design for SOFCs.[8-10] Greene et al.[8] investigated an electrode with a functionally graded porosity distribution in one dimension with the mean-transport pore model to approximate the geometry of a porous media. Results showed that increasing the electrode porosity near the electrolyte will improve the cell performance for certain fuels. Ni et al.[9] studied the particle size gradient using one-dimensional modeling and consequently porosity gradient effects on SOFC performance. The results demonstrated that while this design could significantly enhance the gas transport for thick electrodes, too much gradient for thin electrodes may increase the activation overpotentials. It is also claimed that the particle size gradient is generally more effective than the porosity gradient. Cable and Sophie[10] created a symmetrical, bielectrode supported cell, where the functionally graded porous electrodes were fabricated using the freeze tape casting technique. Recently, we developed a comprehensive SOFC model to study functionally graded electrodes in a general sense.[11] Results indicate that a suitable microstructure design of electrodes may significantly improve SOFC performance.

While functionally graded electrode may provide great potentials to improve SOFC performance, these designs are essentially ad hoc, where the porosity and particle size of electrodes are assumed empirically. It is well known that very complicated multi-physicochemical processes are involved in functional electrodes; consequently, very strong interdependency exists among heat transfer, fuel/gas transport, charge migration, and electrochemical reactions. The improvement of one aspect does not necessarily lead to the improvement for others; on the contrary, it may cause performance deterioration for others. For example, better mass transport performance, e.g., large porosity of electrodes, may cause performance decrease for charge conductivity of porous networks and the effective triple phase boundary length. While the dense electrode design may improve the conductivity for the charge transport, it will inevitably lead to the increased mass transport loss. The competing nature of these properties imposes a great challenge on suitable electrode designs. Especially, SOFC performance is nonlinearly dependent on multiparameters associated with the electrodes.

In this paper, a systematic design method is developed to tune the porosity and particle diameter distributions of electrodes so that the overall SOFC performance can be optimized. In particular, an SOFC model is established to link the electrode property (parameters associated with electrode) with a design objective function (cell performance). A genetic algorithm is employed to systematically search a design space according to the model development. A proton conducting button cell is utilized as an example to demonstrate the optimization approach.

Mathematical Modeling

The SOFC model development is based on the experimental setup as shown in Fig. 1. An anode-supported button cell is mounted on one end of a large ceramic tube. The mixture of hydrogen and vapor as fuel is supplied to the anode electrode via a small ceramic tube. The surplus gas will flow out through the large ceramic tube. The cathode electrode is exposed to ambient air. A tube furnace is used to control the temperature of the cell test stand. Due to the axial symmetry, two-dimensional computational domain is employed and a proton conducting SOFC NiO-BZCY7/BZCY7/BZCY7-GBCF[12] is employed as a physical base for the model development. In order to keep the conciseness and compactness of the paper, the mathematical model is summarized in Table I. The detailed SOFC modeling approach can be found in our recent paper.[11] The model associated parameters are characterized in Table II.

Model Validation

The mathematical model presented in this paper is solved using the finite element package COMSOL MULTIPHYSICS version 3.5a. For a specified cell voltage at anode electrode boundary, the corresponding cell average current density is calculated. The cell polarization curve is then obtained by specifying a series of cell voltages and calculating the corresponding average current densities.

[z] E-mail: Xue@cec.sc.edu

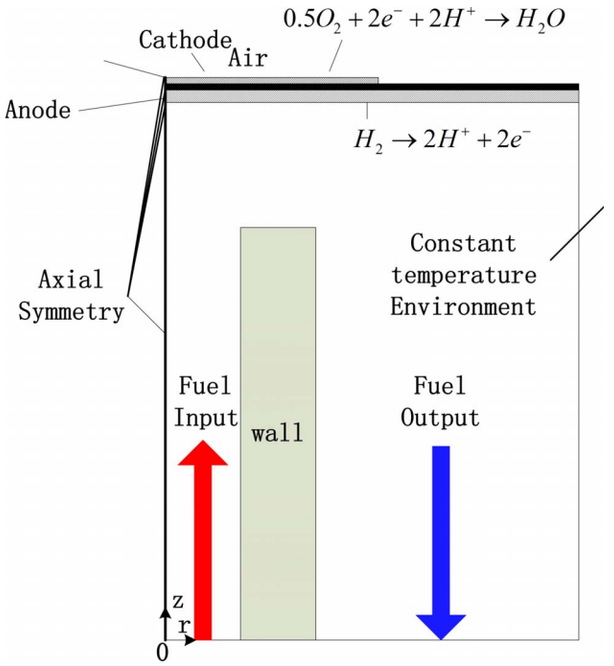

Figure 1. (Color online) Schematic of an experimental SOFC button cell.

Model validation with experimental results is very useful to test model behavior upon the variation of physical parameters. For this purpose, we measured polarization performance of an in-house made button cell (NiO-BZCY7/BZCY7/BZCY7-GBCF) consisted of a ~650 μm thick NiO-BZCY7 anode-supported layer with relatively large porosity, an ~80 μm NiO-BZCY7 anode functional layer with relatively small porosity, an ~20 μm thick BZCY7 electrolyte membrane, and an ~15 μm GBCF + BZCY7 cathode layer. The cell was tested from 600 to 700°C with humidified hydrogen (~3% H_2O) as fuel and the static air as oxidant.[12] The experimental result is shown in Fig. 2. The physical parameters used in the model validation are shown in Table III. The parameters with "*" are difficult to determine in the experiment and are used as adjustable parameters to fit the model predictions with the experimental results. The comparison results are shown in Fig. 2. It can be seen that the numerical results agree reasonably well with the experimental results.

Electrode Optimization via Genetic Algorithm

The validated SOFC model then can be employed to improve/optimize the cell performance. This task is generally performed through parameter study in literature, where the design parameters are varied in certain ranges and the cell performance is examined accordingly. The parameters corresponding to the best cell performance are claimed as the desired design parameters. However, this parameter sweeping design method might be only applicable for relatively simple cases with a couple of design parameters. Considering the multidesign parameters of SOFC electrodes, it will be extremely difficult for such a design method to single out the design parameter values corresponding to the optimal cell performance, where the design space defined by multiparameters is multidimensional, the design solutions induced by the combination of these parameters could be infinite.

In this paper, a genetic algorithm is employed to design electrodes through the effective searching of the design space so that the cell performance can be maximized. Genetic algorithm is an adaptive optimization strategy and is used to search the design space according to the principle of natural selection and the survival of the fittest. Figure 3 illustrates the SOFC electrode optimization procedure using a genetic algorithm. The initial population (electrode design) is generated either randomly or empirically. Each individual in the population represents a possible solution (e.g., distributions of porosity and particle size for electrode) in the design space and is generally called a chromosome; the design solution is described by a binary code. For each individual, their corresponding objective function (e.g., cell polarization performance) is calculated using the

Table I. Mathematical model.[11]

Governing equations	Mathematical expressions	
Charge conservation (electron)	$\begin{cases} \text{Anode electrode layer: } \nabla\,(\sigma_a^{\text{eff}}\,\nabla\,\phi_e) = -\,j_a S_{\text{TPB}} \\ \text{Cathode electrode layer: } \nabla\,(\sigma_c^{\text{eff}}\,\nabla\,\phi_e) = -\,j_c S_{\text{TPB}} \end{cases}$	[1]
Charge balance (proton)	$\begin{cases} \text{Electrolyte layer: } \nabla\,(\kappa\,\nabla\,\phi_p) = 0 \\ \text{Anode electrode layer: } \nabla\,(\kappa_a^{\text{eff}}\,\nabla\,\phi_p) = j_a S_{\text{TPB}} \\ \text{Cathode electrode layer: } \nabla\,(\kappa_c^{\text{eff}}\,\nabla\,\phi_p) = j_c S_{\text{TPB}} \end{cases}$	[2]
Mass conservation	$\nabla\left(\rho\mathbf{u}\omega_i - \rho\omega_j \Sigma D_i^{\text{eff}}\left(\nabla\,x_i + (x_i - \omega_j)\frac{\nabla p}{p}\right)\right) = S_i$	[3]
Momentum conservation	$\text{Channel:}\begin{cases} \rho(\mathbf{u}\,\nabla)\mathbf{u} = \nabla\left(-p\mathbf{I} + \mu\left[\left[\nabla\,\mathbf{u} + (\nabla\,\mathbf{u})^T\right] - \frac{2}{3}(\nabla\,\mathbf{u})\mathbf{I}\right]\right) \\ \nabla(\rho\mathbf{u}) = 0 \end{cases}$	[4]
	$\text{Electrode:}\begin{cases} \left(\frac{\mu}{K} + S_m\right)\mathbf{u} = \nabla\left(-p\mathbf{I} + \frac{\mu}{K}\left[\left[\nabla\,\mathbf{u} + (\nabla\,\mathbf{u})^T\right] - \frac{2}{3}(\nabla\,\mathbf{u})\mathbf{I}\right]\right) \\ \nabla(\rho\mathbf{u}) = S_m \end{cases}$	
Energy conservation	$\nabla\left(k\,\nabla\,T + \sum_i h_i \mathbf{n}_i\right) + \rho C_p u\,\nabla\,T = S_h^e + S_h^j$	[5]

Table II. Model parameter characterization.[11]

Volumetric current densities	$\begin{cases} j_a = j_{0,\mathrm{ref}}^{\mathrm{H_2}}\left[\dfrac{c_{\mathrm{H_2}}}{c_{\mathrm{H_2,bulk}}}\exp\left(\dfrac{\alpha n F\eta_a}{RT}\right) - \exp\left(-\dfrac{(1-\alpha)nF\eta_a}{RT}\right)\right] \\ j_c = j_{0,\mathrm{ref}}^{\mathrm{O_2}}\left[\dfrac{c_{\mathrm{O_2}}}{c_{\mathrm{O_2,bulk}}}\exp\left(\dfrac{\alpha n F\eta_c}{RT}\right) - \dfrac{c_{\mathrm{H_2O}}}{c_{\mathrm{H_2O,bulk}}}\exp\left(-\dfrac{(1-\alpha)nF\eta_c}{RT}\right)\right] \end{cases}$	[6]
Cathode exchange current density	$j_{0,\mathrm{ref}}^{\mathrm{O_2}} = \dfrac{\beta_{ca}RT}{4F}\exp\left(-\dfrac{E_{\mathrm{act,ca}}}{RT}\right)(p_{\mathrm{O_2,ca}})^{0.25}$	[7]
Anode exchange current density	$j_{0,\mathrm{ref}}^{\mathrm{H_2}} = \dfrac{\beta_{an}RT}{4F}\exp\left(-\dfrac{E_{\mathrm{act,an}}}{RT}\right)(p_{\mathrm{H_2,an}})^{0.25}$	[8]
Activation overvoltage	$\eta_i = \phi_e - \phi_i - \Delta\phi_{\mathrm{eq}}$	[9]
Effective ionic conductivity	$\sigma_{\mathrm{eff}} = \kappa[\varphi(1-\varepsilon)P_{\mathrm{el}}]^m$	[10]
Effective electronic conductivity	$\kappa_{\mathrm{eff}} = \kappa[(1-\varphi)(1-\varepsilon)P_{io}]^m$	[11]
Probability for i-phase particles	$P_i = \left[1 - \left(\dfrac{4.236 - Z_{i-i}}{2.472}\right)^{2.5}\right]^{0.4}$	[12]
Volumetric reactive surface area	$S_{\mathrm{TPB}} = \pi\sin^2(\theta_c)N_t d_{\mathrm{el}} d_{io} n_{\mathrm{el}} n_{io} P_{io} P_{\mathrm{el}} \dfrac{Z_{\mathrm{el}} Z_{io}}{Z}$	[13]
Coordination number	$Z_{i-j} = n_j \dfrac{Z_i Z_j}{Z} Z_{\mathrm{el}} = 3 + \dfrac{Z-3}{n_{\mathrm{el}} - (1-n_{\mathrm{el}})\left(\dfrac{d_{io}}{d_{\mathrm{el}}}\right)^2}$ $Z_{io} = 3 + \dfrac{Z-3}{n_{\mathrm{el}}\left(\dfrac{d_{\mathrm{el}}}{d_{io}}\right)^2 - (1-n_{\mathrm{el}})}$	[14]
Number fraction	$n_{\mathrm{el}} = \dfrac{\left(\dfrac{d_{io}}{d_{\mathrm{el}}}\right)^3 \varphi_{\mathrm{el}}}{1 - \varphi_{\mathrm{el}} + \left(\dfrac{d_{io}}{d_{\mathrm{el}}}\right)^3 \varphi_{\mathrm{el}}} n_{io} = 1 - n_{\mathrm{el}}$	[15]
Number density of all particles	$N_t = \dfrac{1-\varepsilon}{\left(\dfrac{4\pi}{3}\right)d_{\mathrm{el}}^3\left(n_{\mathrm{el}} + (1-n_{\mathrm{el}})\left(\dfrac{d_{io}}{d_{\mathrm{el}}}\right)^3\right)}$	[16]
Effective diffusion coefficient	$D_{ij}^{\mathrm{eff}} = \dfrac{\varepsilon}{\tau}\left(\dfrac{D_{ij}D_{\mathrm{Kn},i}}{D_{ij} + D_{\mathrm{Kn},i}}\right)$	[17]
Binary diffusivity coefficient	$D_{ij} = \dfrac{1.43e^{-8}T^{1.75}}{pM_{ij}^{1/2}(v_i^{1/3} + v_j^{1/3})}$	[18]
Mean molecular mass	$M_{ij} = \dfrac{2}{\dfrac{1}{M_i} + \dfrac{1}{M_j}}$	[19]
Knudsen diffusion coefficient	$D_{\mathrm{Kn},i} = \dfrac{97}{2} d_{\mathrm{pore}} \sqrt{\dfrac{T}{M_i}}, d_{\mathrm{pore}} = \dfrac{2}{3}\dfrac{\varepsilon}{1-\varepsilon} d_p$	[20]
Average molecular weight	$M = \sum_{j=1}^{n} x_j M_j$	[21]
Density	$\rho = \dfrac{pM}{RT}$	[22]
Permeability	$K = \dfrac{\varepsilon^3 d_p^3}{180\tau(1-\varepsilon)^2}$	[23]
Mass source term	$S = \sum_i \dfrac{j_i M_i}{n_i F} \quad S_m = \sum_i S_{\mathrm{TPB}} \dfrac{j_i M_i}{n_i F}$	[24]
Heat source term	$S_h^e = (\Delta E_{\mathrm{elec\text{-}chem}} - \Delta G)\dfrac{j}{n_i F}, S_h^j = \sigma_{io}\varphi_{io}^2$	[25]

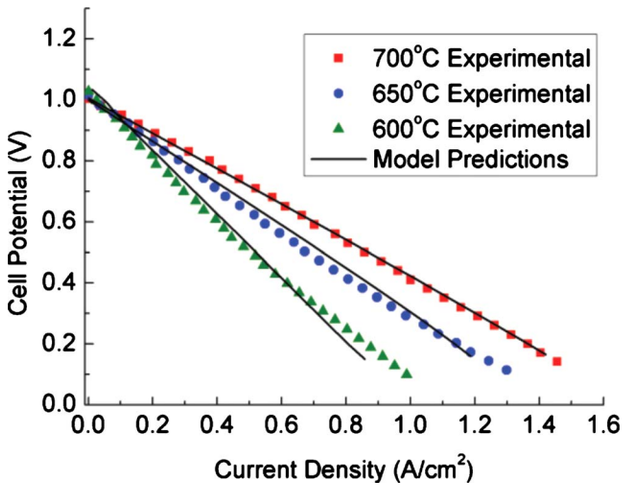

Figure 2. (Color online) Comparisons between simulation results and experimental data.

above SOFC model relating the design solution to the cell performance. Based on the objective function value, the fitness then is assigned for each individual. If stop condition is not satisfied, the procedure will generate new descendents through three step operations, e.g., selection, crossover, and mutation. In the selection step, the parents are selected from the population using a scheme that

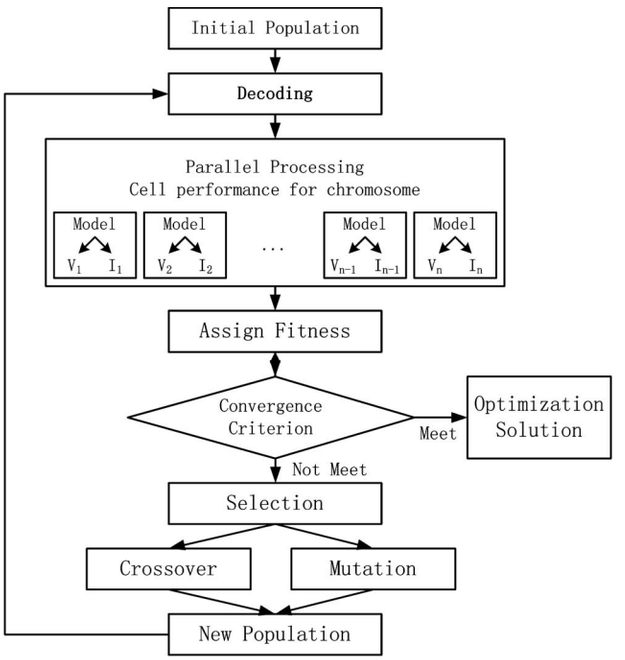

Figure 3. Flow diagram of genetic algorithm.

Table III. Parameters used for SOFC model validation.[3,5-7,11]

Parameter name	Validation	Investigation
Furnace operating temperature, T_{op} (°C)	600/650/700	700
Pressure, p (Pa)	101,325	101,325
Fuel composition, x_{H_2}:x_{H_2O}	0.97:0.03	0.97:0.03/0.5:0.5
Air composition, x_{O_2}:x_{H_2O}:x_{N_2}	0.18:0.03:0.79	0.18:0.03:0.79
Anode conductivity, σ (S/m)	$\left(9.5 \times \frac{10^7}{T}\right)e^{-1150/T}$	$\left(9.5 \times \frac{10^7}{T}\right)e^{-1150/T}$
Cathode conductivity, σ (S/m)	$\left(4.2 \times \frac{10^7}{T}\right)e^{-1200/T}$	$\left(4.2 \times \frac{10^7}{T}\right)e^{-1200/T}$
*Electrolyte conductivity, κ (S/m)	0.19/0.27/0.35	0.35
Electrolyte thickness, l_{el} (μm)	20	20
Anode support layer thickness, l_{sl} (μm)	680	700 (Total thickness)
Anode active layer thickness, l_{al} (μm)	15	
Cathode electrode thickness, l_{ca} (μm)	15	50
Electrolyte and anode radius (cm)	0.5	0.5
Cathode radius (cm)	0.25	0.25
Fuel inlet channel radius (cm)	0.09	0.09
Fuel inlet channel wall radius (cm)	0.035	0.035
Porosity of anode support layer	0.4	0.2–0.6
Porosity of anode function layer	0.2	0.2–0.6
Porosity of cathode	0.35	0.2–0.6
*Tortuosity of anode support layer, τ_{sl}	4.0	$\varepsilon^{-0.5}$
*Tortuosity of anode function layer, τ_{al}	4.0	$\varepsilon^{-0.5}$
*Tortuosity of cathode, τ_c	3.0	$\varepsilon^{-0.5}$
Particle diameter d_p d_{el} d_{io} (μm)	0.25	0.1–1
*Contact angel between e^- and O^{2-} conducting particles θ (°C)	15	15
Volume fraction of e^- conducting particles, φ	0.5	0.5
*β_{ca}	5.76×10^{10}	5.76×10^{10}
*$E_{act,ca}$ (J/mol)	130,000	130,000
*β_{an}	3.39×10^{12}	3.39×10^{12}
*$E_{act,an}$ (J/mol)	120,000	120,000

Parameters marked with an asterisk (*) are adjustable parameters.

favors the more fit individuals. With the two selected parents, the crossover operation is employed to cut their chromosome strings at a randomly chosen position. The tail segments are then swapped over to form two offspring. The mutation operation is then applied to each child individually after crossover, and randomly alters each gene (bit of coding string) with a small probability. It is generally recognized that the crossover may rapidly explore the design space while the mutation provides a small amount of random search and ensures that every point in the design space has probability to be examined.[13-15] With new descendents, the procedure performs the next iteration of the search until the optimal design solution is obtained.

In order to perform the optimization design, both the electrode porosity and the particle size are represented using graded functions in a general sense[11]

$$\varepsilon_i(Z) = 0.4Z^{\lambda_i} + 0.2 \qquad Z \in [0,1] \quad i = \text{a,c} \quad \lambda_i \in [0.1,20] \tag{26}$$

$$d_i(Z)[\mu\text{m}] = 0.9Z^{\xi_i} + 0.1 \qquad Z \in [0,1] \quad i = \text{a,c} \quad \xi_i \in [0.1,20] \tag{27}$$

where subscripts a and c represent anode and cathode, respectively; Z is a dimensionless parameter measuring the distance between the electrode/electrolyte interface (corresponding to value 0) and the electrode/gas channel interface (corresponding to value 1); λ and ξ are variables defining the shape of graded porosity and particle size distributions. The distributions defined by Eq. 26 and 27 can be parabolic, linear, and inverse parabolic. As a result, the porosity and particle size monotonically increase from the electrode/electrolyte interface toward the electrode/channel interface. This idea is inspired by the functionally graded electrodes fabricated using the freeze tape casting technique,[10] where the porosity reaches the minimum value at the electrode/electrolyte interface while reaching the maximum value at the electrode/channel interface. The porosity and particle size are dependent on the specific fabrication processes. The upper and lower bounds are established based on the fundamental physical considerations. For example, the electrode with too high porosity might not be practical, so the upper bound 0.6 is chosen in this paper; considering the functionally graded design, the lower porosity bound less than the upper bound is needed, e.g., 0.2. The particle size is dependent on the specific synthesis process, here the bound (0.1 μm, 1 μm) is chosen. For practical designs using the proposed method, these parameters can be adjusted according to the specific synthesis/fabrication processes. The purpose of the design is to search for suitable combinations of porosity and particle size distributions via a genetic optimization algorithm so that the cell performance is maximized.

Two issues need to be solved for genetic algorithm implementation: one is the genetic representation of the design variables; another one is the definition of fitness function measuring the quality of the represented solution. According to Eq. 26 and 27, λ and ξ are the design variables. To implement the genetic representation of design solution, the following transformation is employed

$$\begin{cases} \lambda_i = \dfrac{pr_\lambda}{255}(\lambda_{i,\max} - \lambda_{i,\min}) + \lambda_{i,\min} \\ \xi_i = \dfrac{pr_\xi}{255}(\xi_{i,\max} - \xi_{i,\min}) + \xi_{i,\min} \end{cases} \tag{28}$$

where $\lambda_{i,\max}$ and $\lambda_{i,\min}$ are the maximal and minimal values of λ_i, and $\xi_{i,\max}$ and $\xi_{i,\min}$ are the maximal and minimal value of ξ_i, respectively. The "pr" is an eight-bit binary code string representing the corresponding decimal values of λ and ξ. For an eight-bit binary code string, the maximum value is (11111111) and the minimum value is (00000000), and when transformed into decimal numbers, the values are 255 and 0, respectively. As a result, the pr variation between (00000000) and (11111111) in the binary code format is equivalent to the pr variation between 0 and 255 in the decimal format. A eight-bit code can approach to a precision of 4×10^{-3}; therefore, the relative error of λ_i (or ξ_i) expression is less than 1% in this paper.[16,17] During the searching procedure of optimal solutions, Eq. 28 is utilized for a two-way transformation between λ and ξ and their corresponding eight-bit binary codes. The values of λ and ξ are used for the SOFC model to calculate the objective/fitness functions, while their corresponding eight-bit binary codes are utilized for the operations of the genetic algorithm.

Because the purpose of the optimization is to maximize the cell performance, the cell average current density is employed as the fitness/objective function as shown in Eq. 29, where the summation of the cell current densities under the concerned cell voltage range will be maximized. In Eq. 29, j is the average current density of the cell and M is a constant coefficient used to facilitate the calculation of genetic algorithm optimization

$$\text{fitness} = M \times \sum_{V_{\text{cell}}} j_{V_{\text{cell}}} \tag{29}$$

The genetic algorithm is implemented using the in-house developed code. The SOFC simulation is embedded into the optimization loop for optimal solution searching. Due to the global property of genetic algorithm,[13] the initial population to start the algorithm is randomly selected within the bounds in Eq. 26 and 27.

Results and Discussion

For the design of electrodes, the combination of both the particle size and the porosity is optimized. The basic physical parameters of the model are shown in Table III. Four cases are considered and compared, including homogeneous particle diameter and graded porosity (case I: homo-d_p, heter-ε), graded particle diameter and homogeneous porosity (case II: heter-d_p, homo-ε), homogeneous particle diameter and porosity (case III: homo-d_p, homo-ε), and graded particle diameters and graded porosity (case IV: heter-d_p, heter-ε). The general graded porosity and graded particle diameter are represented using Eq. 26 and 27, respectively. For homogeneous case, the porosity and particle diameter are uniform, e.g.

$$\varepsilon_i = \lambda_i \quad i = \text{a,c} \quad \lambda_i \in [0.2,0.6] \tag{30}$$

$$d_i[\mu\text{m}] = \xi_i[\mu\text{m}] \quad i = \text{a,c} \quad \xi_i \in [0.1,1.0] \tag{31}$$

In the experimental setup shown in Fig. 1, the cathode is exposed to air, the humidified hydrogen is supplied to the anode through a small ceramic tube. In optimization designs, three fuel compositions at the inlet of fuel supply tube are assumed; i.e., the molar ratio of hydrogen to vapor is chosen as 0.97:0.03, 0.6:0.4, and 0.4:0.6, respectively. Using optimization procedure illustrated in Fig. 3, we perform electrode designs according to Eq. 26, 27, 30, and 31. The history of fitness value evolution is shown in Fig. 4. The vertical axis is the fitness while the horizontal axis is the number of iteration times. It can seen that the fitness reaches a stable value for each of the four design cases after about 500 times iteration and the genetic algorithm converges.

The corresponding optimization results of the cell performance are shown in Fig. 5. When the inlet molar ratio of hydrogen to vapor is relatively high (H_2/H_2O = 0.97:0.03), the performances of the cell with different electrode designs are quite similar to each other as shown in Fig. 5a. At a high cell current density, the cell performance shows a slight difference. When the fuel composition at the inlet of supply tube changes to H_2/H_2O = 0.6:0.4, the cell performance comparison is shown in Fig. 5b. It is obvious to see that the cell performance difference is significant when the current density is beyond ~3700 A/m^2. The performance of the cell with homogeneous electrode design (uniform particle size and uniform porosity distribution) is the worst one, while the cell with heterogeneous electrode design obtains the best performance and is quite close to case II electrode design (heterogeneous particle size and homogeneous porosity). The performance of the cell with case I electrode design (homogeneous particle size and heterogeneous porosity distribution) is in between. It is worth mentioning that even though the

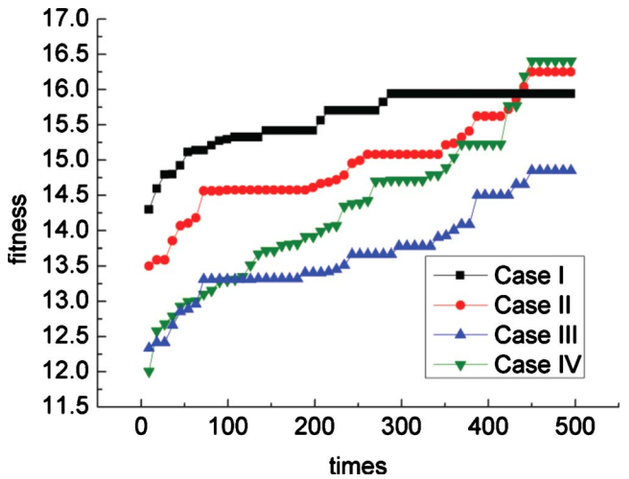

Figure 4. (Color online) Fitness evolutions in optimization process.

cell with homogeneous electrode design has the worst performance, it is the best performance we can obtain using the optimization algorithm when the homogeneous electrode is assumed. When the fuel composition at the inlet of the supply tube changes to H_2/H_2O = 0.4:0.6, the optimized cell performances are shown in Fig. 5c. The cell performance shows a similar trend to those shown in Fig. 5b; however, the performance starts to deviate from each other beyond the current density of about 2500 A/m^2, and the difference becomes increasingly significant when comparing the homogeneous electrode design (case III: uniform particle size and uniform porosity) to the rest of electrode designs. One may notice that the optimization results are dependent on the operating conditions, e.g., fuel composition at the inlet of supply tube. One may also notice that the cell with heterogeneous electrode design (case IV) obtains the best performance, while that with homogeneous electrode design (case III) has the worst performance. The graded electrode design may effectively improve the cell performance under the conditions of the high current density and the low ratios of hydrogen to vapor. In all of the three fuel composition conditions, the electrode design with heterogeneous particle size and homogeneous porosity (case II) obtains a similar cell performance to that with heterogeneous particle and porosity (case IV), indicating that the graded particle size has more potentials to improve the cell performance than the graded porosity in the present system settings.

The corresponding electrode (anode and cathode) design results are detailed in Table IV for different fuel compositions. For homogeneous porosity (cases I, II, and III), the optimized value consistently reaches the specified low limit porosity of 0.2 for the cathode; the optimized porosity for the anode reaches the specified high limit value of 0.6 with an exception of case III under the fuel composition of H_2/H_2O = 0.97:0.03, where the optimized porosity is 0.451 as shown in Table IV. In the anode-supported SOFC, the anode electrode is much thicker than the cathode electrode, consequently, the high porosity for the former facilitates the fuel diffusion; however, the low porosity for the cathode indicates that the gas diffusion resistance is not a major hurdle for the thin cathode in this work. For homogeneous particle size cases (cases I and III), the optimized diameter unanimously reaches the specified low limit value of 0.1 μm for the cathode and anode with homogeneous porosity. When the heterogeneous porosity is employed for the anode (case I), the optimized particle diameter is dependent on the fuel composition. When the ratio of hydrogen to vapor is relatively high

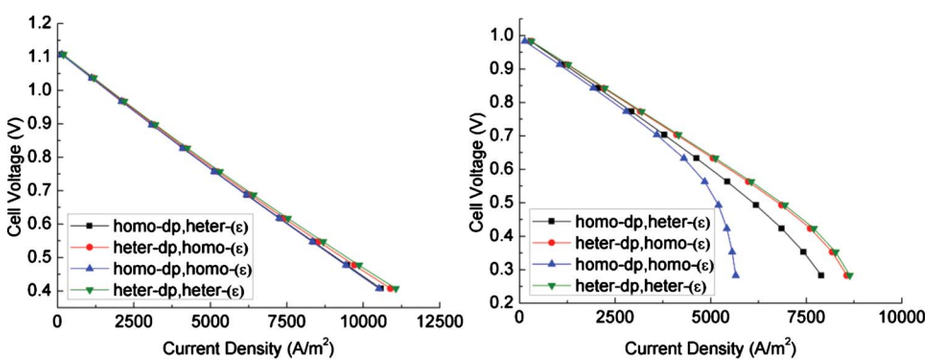

(a) $x_{H_2}(0.97) : x_{H_2O}(0.03)$ (b) $x_{H_2}(0.6) : x_{H_2O}(0.4)$

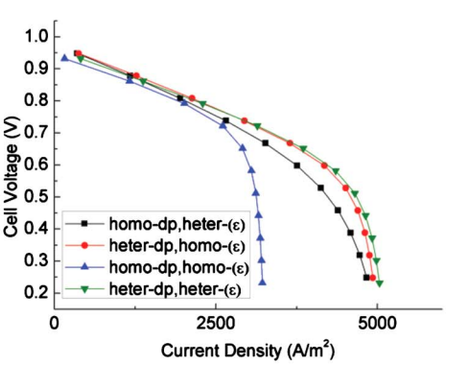

(c) $x_{H_2}(0.4) : x_{H_2O}(0.6)$

Figure 5. (Color online) Optimized cell performances with different inlet fuel compositions.

Table IV. Optimization results.

(a) Optimization results with $x_{H_2}(0.97):x_{H_2O}(0.03)$

Case	λ_a	λ_c	ξ_a	ξ_c
I: homo-d_p, heter-ε	0.373	20	0.1	0.1
II: heter-d_p, homo-ε	0.6	0.2	1.932	20
III: homo-d_p, homo-ε	0.451	0.2	0.1	0.1
IV: heter-d_p, heter-ε	0.375	20	1.683	20

(b) Optimization results with $x_{H_2}(0.6):x_{H_2O}(0.4)$

Case	λ_a	λ_c	ξ_a	ξ_c
I: homo-d_p, heter-ε	0.341	20	1	0.1
II: heter-d_p, homo-ε	0.6	0.2	1.124	20
III: homo-d_p, homo-ε	0.6	0.2	0.1	0.1
IV: heter-d_p, heter-ε	0.1	20	1.069	20

(c) Optimization results with $x_{H_2}(0.4):x_{H_2O}(0.6)$

Case	λ_a	λ_c	ξ_a	ξ_c
I: homo-d_p, heter-ε	0.195	20	1	0.1
II: heter-d_p, homo-ε	0.6	0.2	0.897	20
III: homo-d_p, homo-ε	0.6	0.2	0.1	0.1
IV: heter-d_p, heter-ε	0.1	20	0.877	20

(0.97:0.03), the optimized particle diameter is still 0.1 μm. When the ratio of hydrogen to vapor reduces to a relatively low value, e.g., 0.6:0.4 and 0.4:0.6, the optimized particle diameter raises to 1 μm.

In the case of graded electrode designs, the results listed in Table IV for the anode electrode are visualized in Fig. 6, including the graded porosity (Fig. 6a through 6c) and the graded particle size (Fig. 6d through 6f). When the fuel composition at the inlet of fuel supply tube is set at H_2/H_2O = 0.97:0.03, the optimization result of the anode porosity distribution is identical for case I (homogeneous particle size and heterogeneous porosity) and Case IV (heterogeneous particle size and heterogeneous porosity) as shown in Fig. 6a. The corresponding optimized particle size distribution for case IV is shown in Fig. 6d, which is different from the optimized homogeneous particle size for case I. This difference drives a slight distinction of the cell performance for case I and case IV as shown in Fig. 5a. When the ratio of hydrogen to vapor at the inlet raises to 0.6:0.4 and 0.4:0.6, the optimization results of Case IV are shown in Fig. 6b and 6c for the porosity distributions and in Fig. 6e and 6f for the particle size distributions. Because both porosity and particle size distributions of Case IV are different from those of Case I, the differences of corresponding cell performances shown in Fig. 4b and 4c become significant. The comparisons of case II (heterogeneous particle size and homogeneous porosity) with case IV are shown in Fig. 6e and 6f. Under the different inlet fuel composition settings, the optimized particle size distributions are almost identical. Although the porosity distributions for case II and case IV are totally different, the corresponding cell performance is very close to each other as shown in Fig. 4a through 4c. This observation again indicates that the particle size gradient is more effective than the porosity gradient in cell performance improvement in the present system settings.

For the graded cathode design, the optimized design parameters λ and ξ unanimously reach the maximum value of 20. Considering Eq. 26 and 27, we can see that the porosity and particle size distributions are approximately uniform with values of 0.2 and 0.1 μm, respectively. In the anode-supported SOFCs, the cathode layer is very thin. The path of the oxygen (air) transport from the surrounding atmosphere to the reaction sites is very short. Additionally, the free air breathing is employed for the gas supply at the cathode side in the current physical settings. Consequently, the functionally graded distributions do not play critical roles in this case. Instead, the fine particle size and the small porosity will increase the effective reaction area and facilitate the cell performance improvement. These are the reasons that the optimized cathode property approaches uniform and reaches the minimum bound (0.2 for the porosity and 0.1 μm for the particle size) even though the graded cathode is assumed for the optimization process.

According to the optimized electrodes in Table IV, the corresponding hydrogen molar fraction distribution is further examined, where the operating condition for the cell with the inlet fuel composition of H_2/H_2O = 0.6:0.4 and the cell voltage of 0.4 V is chosen as an example. Figure 7 shows the hydrogen molar fraction distributions with different electrode (anode and cathode) designs. Essentially the hydrogen molar fraction decreases from the inlet toward the anode/electrolyte interface. The gradient of hydrogen molar fraction distribution is induced by the combinational effects of electrochemical reaction and diffusion resistance. The lower hydrogen molar fraction in the anode will result in the higher concentration overpotential loss. From Fig. 7, one can see that the case III design

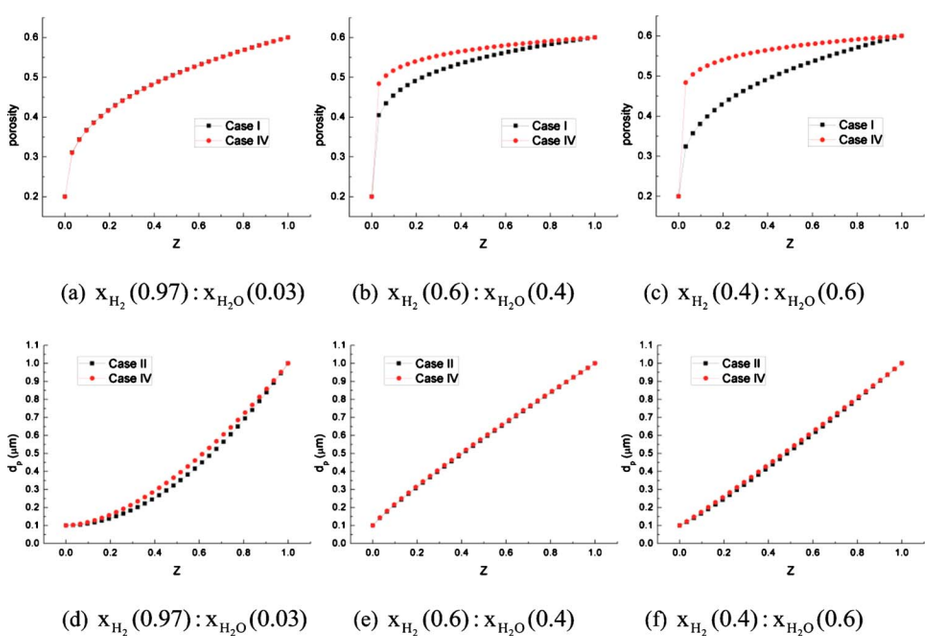

Figure 6. (Color online) Anode porosity distribution of cases I and IV [(a)–(c)] and particle diameter distribution of cases II and IV [(d)–(f)].

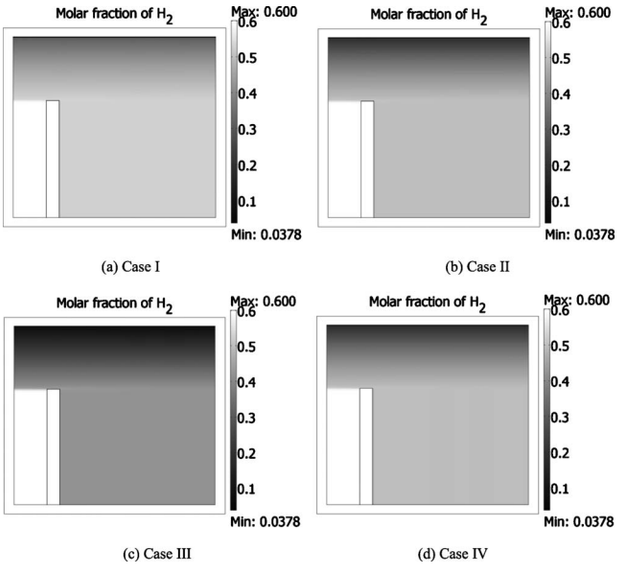

Figure 7. Hydrogen molar fraction distributions under the operating conditions with the inlet fuel composition of H_2/H_2O = 0.6:0.4 and the cell voltage of 0.4 V.

leads to the highest concentration overpotential loss, this observation is consistent with the cell performance shown in Fig. 4b. Although the cell with the case I design has the highest hydrogen molar fraction within the anode, the corresponding performance is not the best one (Fig. 4b). Other parameters such as particle size also affect the electrode property and consequently the cell performance. This result further confirms the previous understanding that the electrode property is determined by several competing parameters. The hydrogen molar fraction distributions in Fig. 7b and 7d can be similarly interpreted.

Conclusions

A comprehensive mathematical model of anode-supported SOFC integrated with a fuel supply tube is presented. The model is validated using the experimental results of a proton conducting SOFC (NiO-BZCY7/BZCY7/BZCY7-GBCF) under different operating conditions. Based on the model development, a genetic optimization method is employed to design the electrodes (anode and cathode) so that the cell performance is maximized. Results indicate that the optimization results of graded electrodes may obtain the best cell performance while those of homogeneous electrodes obtain the worst cell performance. The graded particle size distribution is more effective than the graded porosity distribution on the cell performance improvement. The optimization results are dependent on the cell operating conditions. For the anode-supported SOFC with free-air breathing conditions, the optimized cathode properties tend to be uniform with the minimum particle size and minimum porosity.

Acknowledgment

This work is supported by the U.S. Department of Energy under grant no. DE-SC0001061 through the Energy Frontier Research Center (EFRC) entitled "Science Based Nanostructure Design and Synthesis of Heterogeneous Functional Materials for Energy Systems."

University of South Carolina assisted in meeting the publication costs of this article.

List of Symbols

c_i concentration of species i
d_p particle diameter in porous electrode, m
d_{pore} pore diameter in porous electrode, m
D_{ij} binary mass diffusion coefficient of a mixture species i and j, $m^2\ s^{-1}$
D_{ij}^{eff} effective diffusion coefficient, $m^2\ s^{-1}$
$D_{Kn,i}$ Knudsen diffusion coefficient of species i, $m^2\ s^{-1}$
E Activation energy, J mol^{-1}
F Faraday's constant: 96,487, C mol^{-1}
h enthalpy
$\mathbf{I}$ identity matrix
j_i current density, A m^{-2}
j_0 exchange current, A m^{-2}
K permeability of porous electrode, m^2
k Thermal conductivity, W $m^{-1}\ K^{-1}$
M average molecular weight, kg mol^{-1}
M_{ij} mean molecular mass
$\mathbf{n}_i$ molar flux vector
n_i Number fraction
N_t number density of all particles, m^{-3}
p pressure, Pa
P_i probability for i phase particles to form percolated or globally continuous clusters
R universal gas constant, J $mol^{-1}\ K^{-1}$
S_h^e heat generation due to electrochemical reaction, W m^{-3}
S_h^j heat generation due to Joule heating, W m^{-3}
S_i reaction source term for species i, kg $m^{-3}\ s^{-1}$
S_m mass source term, kg $m^{-3}\ s^{-1}$
S_{TPB} volumetric reaction surface area, m^{-1}
T temperature, K
$\mathbf{u}$ fluid velocity, m/s
v diffusion volume of gas
V potential, V
x_i mole fraction of species i
y direction perpendicular to electrolyte layer, m
Z_i total coordination for i phase particles
Z total average coordination number

Greek

α electron transfer coefficient (usually 0.5)
β tuning parameter, $\Omega^{-1}\ m^{-2}$
ε porosity
η overpotential, V
κ protonic conductivity, S m^{-1}
λ optimization variable
ξ optimization variable
π ratio of the circumference of a circle to its diameter
ρ density, kg m^{-3}
σ electronic conductivity, S m^{-1}
τ tortuosity
ϕ potential, V
φ volume fraction of electron conducting particles
ω_i weight fraction of species i

Subscripts

a anode
c cathode
el electronic
eq equilibrium
i species i
pol polarization
pro protonic
ref reference
st perturbation
st static
t transient

Superscripts

eff effective

References

1. M. Suzuki and T. Oshima, *Powder Technol.*, **35**, 159 (1983).
2. S. Sunde, *J. Electrochem. Soc.*, **143**, 1123 (1996).
3. P. Costamagna, P. Costa, and V. Antonucci, *Electrochim. Acta*, **43**, 375 (1998).
4. M. M. Hussain, X. Li, and I. Dincer, *J. Power Sources*, **161**, 1012 (2006).
5. M. Ni, M. K. H. Leung, and D. Y. C. Leung, *Energy Convers. Manage.*, **48**, 1525 (2007).
6. D. H. Jeon, J. H. Nam, and C. J. Kim, *J. Electrochem. Soc.*, **153**, A406 (2006).
7. J. H. Nam and D. H. Jeon, *Electrochim. Acta*, **51**, 3446 (2006).
8. E. S. Greene, W. K. S. Chiu, and M. G. Medeiros, *J. Power Sources*, **161**, 225 (2006).
9. M. Ni, M. K. H. Leung, and D. Y. C. Leung, *J. Power Sources*, **168**, 369 (2007).

10. T. T. Cable and S. W. Sofie, *J. Power Sources*, **174**, 221 (2007).
11. J. Shi and X. Xue, *Electrochim. Acta*, **55**, 5263 (2010).
12. H. Ding and X. Xue, *J. Alloys Compd.*, **496**, 683 (2010).
13. J. Holland, *Adaptation in Natural and Artificial Systems*, University of Michigan Press, Ann Arbor, MI (1975).
14. T. D. Gwiazda, in *Genetic Algorithms Reference*, Vol. 1, *Crossover for Single-Objective Numerical Optimization Problems*, Tomasz Gwiazda, Poland (2006).
15. T. D. Gwiazda, in *Genetic Algorithms Reference*, Vol. 2, *Mutation Operator for Numerical Optimization Problems*, Tomasz Gwiazda, Poland (2007).
16. P. Wildi-Tremblay and L. Gosselin, *Int. J. Heat Mass Transfer*, **50**, 464 (2007).
17. J. Shi and J. Wang, *Int. J. Therm. Sci.*, **47**, 1595 (2008).